

Chapter 15

Cubic GaN on Nanopatterned 3C-SiC/Si (001) Substrates

Ricarda Maria Kemper, Donat Josef As and Jörg K. N. Lindner

Abstract In this chapter we demonstrate the growth and characterization of nonpolar relaxed cubic GaN by plasma-assisted molecular beam epitaxy on prepatterned 3C-SiC/Si (001) substrates. Nanopatterning of 3C-SiC/Si (001) was achieved by two different fabrication techniques: nanosphere lithography (NSL) to generate large-area pattern, and conventional electron beam lithography (EBL) for tailoring particular surface morphologies. Both methods were followed by a lift-off and a reactive ion etching (RIE) process. We analyze the influence of the substrate on the GaN growth and show that it is possible to grow single phase and defect-reduced cubic GaN crystals on 3C-SiC nanostructures. Furthermore cubic GaN/AlN multi-quantum wells were grown on 3C-SiC nanostructures, which is a further step toward nanoscaled device applications.

15.1 Introduction

Wide band-gap materials, especially group III-nitrides like GaN, AlN and InN, have a great potential for optoelectronic and electronic device applications like laser diodes and transistors [1–3]. Up to date there is a huge interest in nitride technologies to fabricate dislocation free epilayers for high-quality GaN-based devices.

Devices show best performance if fabricated on lattice-matched substrates since lattice-mismatch leads to the generation of misfit dislocations at the interface which may cause scattering of charge carriers, limited carrier mobility, nonradia-

R. M. Kemper (✉) · D. J. As · J. K. N. Lindner
Department of Physics, University of Paderborn, Warburger Str. 100, 33098 Paderborn, Germany
e-mail: rkemper@mail.uni-paderborn.de

D. J. As
e-mail: d.as@uni-paderborn.de

J. K. N. Lindner
e-mail: lindner@physik.uni-paderborn.de

tive recombination in optical devices and device heating. However, the choice of suitable substrate materials is limited and thus additional techniques have to be developed to overcome persisting mismatch issues.

One method for the elimination of misfit dislocations is the reduction of the growth area [4]. Defect reduction in mismatched systems was also demonstrated by the theory of nanoheteroepitaxy (NHE), which describes the selective growth on a nanopatterned (10–100 nm) substrate [5]. In contrast to planar heteroepitaxy, NHE includes a partitioning of strain between the epilayer and the substrate and a distribution of the mismatch strain in the epilayer in three dimensions. NHE shows the possibility of growing dislocation free epilayers on nonlattice-matched nanopatterned substrates.

So far the most frequently used material among all group-III nitrides is the hexagonal polytype of GaN. In hexagonal GaN because of the crystal symmetry inherent spontaneous and piezoelectric polarization fields are present along the *c*-axis, which influence device characteristics [6, 7]. Therefore, nonpolar and semi-polar systems have attracted growing interest in the past few years [8]. One method to produce real nonpolar materials is the growth of cubic GaN (*c*-GaN). Although the hexagonal polytype is the thermodynamically favorable phase, it has been shown that there is a narrow window of experimental conditions to achieve the heteroepitaxial growth of *c*-GaN [9]. As there is a shortage in low defect density bulk GaN substrates [10] on which one might grow lattice matched GaN epilayers, the most adequate substrate is cubic silicon carbide 3C-SiC (001) exhibiting a lattice misfit of 3.5%. The dislocation density [11] of *c*-GaN deposited on 3C-SiC (001) by plasma-assisted molecular beam epitaxy (MBE) is $\sim (10^9 - 10^{10})\text{cm}^{-2}$, which is in the order of magnitude of what has been achieved in hexagonal GaN epitaxy a few years ago. First, field effect transistors (FET) [3] and infrared detectors [12] based on *c*-GaN have been successfully realized. However, a reduction of the dislocation density would allow the fabrication of high performance devices.

In this chapter, we will describe current attempts (and obstacles) to improve *c*-GaN growth on 3C-SiC by using nanopatterned surfaces. For this purpose we first briefly introduce the theory of nanoheteroepitaxy before we describe experiments and results. We will demonstrate the growth of nonpolar *c*-GaN by molecular beam epitaxy (MBE) on nanopatterned 3C-SiC/Si (001) substrates with an extremely small content of the hexagonal phase. Nanopatterning of 3C-SiC/Si (001) is achieved either with self-organized colloidal masks or using electron beam lithography. Both processes are followed by a lift-off and a reactive ion etching process. We will then highlight the influence of the 3C-SiC substrate on the selective-area-grown *c*-GaN epilayer [13]. It is shown that *c*-GaN grown on 3C-SiC/Si (001) by MBE forms two types of structural domains which are induced by the substrate. They can be distinguished by their surface facets which are oriented either parallel or perpendicular to the [110] direction. Several independent measurement techniques like electron backscatter diffraction and microphotoluminescence demonstrate the formation of hexagonal inclusions preferentially in one type of domains. Finally, the realization of a complex cubic AlN/GaN multiquantum well layer structure on 3C-SiC nanostructures is demonstrated.

The studies presented here aim to give more insight into the basic growth mechanism of c-GaN on 3C-SiC/Si. They thus may help to improve the structural quality of future electrical and optoelectrical devices based on c-GaN grown on 3C-SiC (001). And they give the opportunity toward the fabrication of nanoscaled devices.

15.2 Theory of Nanoheteroepitaxy

In this section we shall address the possibility to avoid extended defects in heteroepitaxial layers by the use of substrates with tailored surface morphologies. In general there are three basic types of defects in epitaxial c-GaN thin films grown on 3C-SiC (001). The first type is misfit dislocations due to relaxation of a pseudomorphically strained thin layer on the substrate. The second type is dislocations originating in the substrate, which extend into the epilayer. The third type is stacking faults (SFs) on $\{111\}$ planes. A change of the stacking sequence leads to hexagonal inclusions (h-GaN), which locally change the crystal symmetry and result in polar faces. As we will see later in Chap. 6, there are also other defects in the substrate which may adversely affect the epi-growth of c-GaN.

A common method for the elimination of misfit dislocations is the reduction of the growth area [4]. Even the reduction of the growth area in the μm -range reduces the nucleation sites of dislocations and filters substrate defects. Furthermore the probability of defect termination at local free surfaces is increased.

Additional defect reduction mechanisms become available, if the growth area is further reduced, as proposed in the theory of nanoheteroepitaxy (NHE) introduced by Hersee et al. [5]. This theory deals with the growth on nanostructures with a size of 10–100 nm. NHE offers the possibility of growing dislocation free epilayers on nonlattice-matched nanopatterned substrates if the growth areas are sufficiently small. In this case, the mismatch-induced stress leads to a three-dimensional strain partitioned between both, the growing film and the substrate. In consequence, the strain within the growing film can be kept below a threshold at which the strain relaxation by the formation of extended defects becomes energetically favorable.

In order to illustrate the difference between conventional epitaxy and nanoheteroepitaxy, Fig. 15.1 displays a schematic drawing of a planar epilayer and a selective-area-grown epilayer on a patterned substrate. In conventional planar epitaxy, the lattice mismatch at the interface leads to lateral strain in the growing film and in consequence to transversal lattice distortions (in growth direction). In contrast, on a two-dimensionally patterned surface both the substrate and the growing film are not subjected to lateral confinements and therefore a three-dimensional partitioning of the strain in the epilayer and in the substrate and consequently a reduced strain in the epilayer is expected. Calculations of the strain energy by Sun and coworkers [14] have shown that the 3.2% lattice mismatch between hexagonal GaN and hexagonal SiC can be accommodated without defect generation when the substrate nanostructures have a size of about 40 nm. Our studies presented here are based on

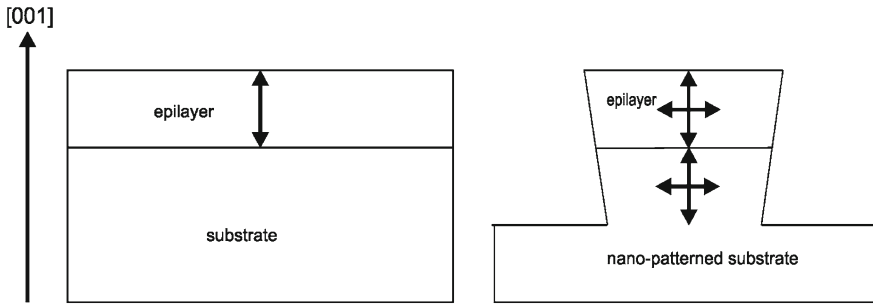


Fig. 15.1 Schematic drawing of a planar epilayer and a selective-area-grown epilayer on a patterned substrate

this theory but use slightly larger surface features. This allows us to observe clearly the structural changes occurring when the three-dimensional growth surfaces instead of planar ones are used.

15.3 Nanopatterning of 3C-SiC

In what follows we shall explain the different basic steps toward the heteroepitaxy of c-GaN by MBE on prepatterned 3C-SiC/Si including the nanopatterning of the substrate. Two techniques are used to obtain nanopatterns on the 3C-SiC/Si (001) substrate: nanosphere lithography (NSL) and electron beam lithography (EBL). Both methods are followed by a lift-off process and reactive ion etching (RIE) process.

15.3.1 Nanopatterning by Nanosphere Lithography

NSL is a cost-effective method to produce regular nanoscale surface patterns of scalable size and with a variety of motifs [15]. NSL uses a self-organized monolayer of nanobeads as a shadow mask in order to create nanopatterns on a surface. The advantage of this technique is that it can easily produce nanopatterns on areas several centimeters large. Therefore, thin film growth studies on NSL-patterned surfaces can subsequently employ all of the standard characterization techniques with typical sampling areas of few millimeters diameter.

3C-SiC (001) thin films grown by chemical vapour deposition on Si (001) [16] were used in our experiments. Due to the hydrophobic character of SiC [17], the substrates were coated with ~ 16 nm of SiO_2 by plasma-enhanced chemical vapor deposition followed by a cleaning process ($\text{H}_2\text{O}:\text{NH}_3:\text{H}_2\text{O}_2 = 3:1:1$). The surface was subsequently covered with a mask of 600 nm diameter polystyrene (PS) spheres forming a self-organized hexagonally closed packed monolayer. This was achieved

by the controlled drying [18] of a droplet of an aqueous suspension of colloidal PS spheres. In the next step, the spheres were shrunk in oxygen plasma as outlined in [19]. On top of the colloidal mask 60 nm of Ni was thermally evaporated and the PS spheres were removed. The resulting Ni-mask-coated 3C-SiC/Si (001) was vertically etched by 300 nm using reactive ion etching (10 % O₂, 6, 1 % SF₆). After removing the metal by FeCl₃ and DI-water (1:3), the samples were cleaned with a buffered oxide etching solution (NH₄F:H₂O:HF = 4:6:1). Altogether, this procedure allows the creation of surface patterns with a lateral feature size of some ten to few hundred nanometers. Figure 15.2 shows a side view scanning electron microscopy (SEM) image of a cleaved nanopatterned 3C-SiC (001) surface. The hole-diameter is about 400 nm and the depth is about 300 nm. Since the cleaving edge cuts through some holes it is obvious that the etching process leads to a high surface roughness at the bottom of the holes.

15.3.2 Nanopatterning by Electron Beam Lithography

EBL is one of the most common techniques to fabricate nanostructure masks. Although for time reasons one would typically fabricate nanostructures only in small areas of few hundred μm^2 , the high flexibility in motive shapes and the excellent precision at which motives can be reproduced make EBL attractive for patterning substrates for selected-area growth studies. Hiller and coworkers [20] have shown how to produce 3C-SiC nanostructures which are aligned parallel to the [110] directions of the substrate. Recently, the same group achieved side wall steepness of up to 83° in 3C-SiC (001) [20].

The used etching masks were formed by EBL and a following lift-off process with a Ni metal mask. The Ni metal mask was produced by thermal evaporation. Due to the high chemical stability of the SiC dry etching techniques are the methods of

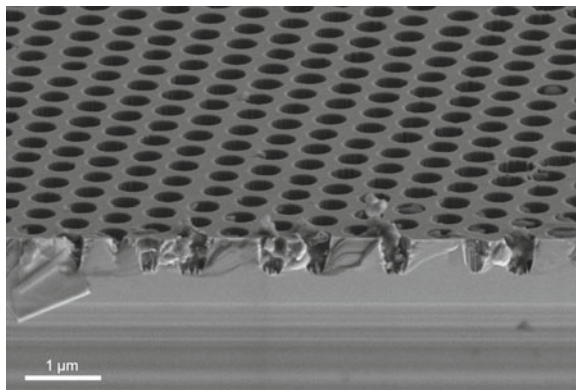
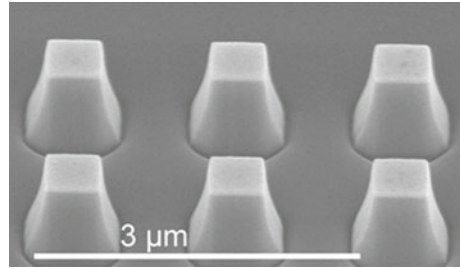


Fig. 15.2 Side view SEM image of a 3C-SiC (001) surface nanopatterned by NSL

Fig. 15.3 Side view SEM image of the 3C-SiC (001) surface with *post-shaped* nanostructures [21]



choice to transfer the mask pattern into the three dimensions. Therefore an electron cyclotron resonance (ECR) plasma system was modified by a special gas inlet unit suitable for injecting SF_6 into the high-density downstream Ar/ O_2 ECR plasma. An etching rate of about 100 nm/min was achieved. Figure 15.3 displays a side view SEM image of the 3C-SiC (001) surface with post-shaped nanostructures. Arrays of 5×5 nanoposts were repeated several times on the substrate surface with etched down spaces in between. The posts have top edges with a length of about 500 nm and a height of about 700 nm.

15.4 Molecular Beam Epitaxy of Cubic GaN

In this section we shall explain the growth of c-GaN on 3C-SiC (001) substrates by MBE. First we will discuss the growth process and the growth parameter of planar c-GaN films. Afterwards the MBE of selective-area-grown c-GaN on prepatterned 3C-SiC/Si (001) is introduced.

15.4.1 Molecular Beam Epitaxy of Planar Cubic GaN Films

Cubic group III-nitride samples were grown on 200 μm thick, free standing 3C-SiC (001) substrates by molecular beam epitaxy (MBE) [22, 23]. An Oxford Applied Research HD25 radio frequency plasma source was used to provide activated nitrogen atoms and gallium was evaporated from a Knudsen cell. Prior to growth, the 3C-SiC substrates were chemically etched by organic solvents and a buffered oxide etch (BOE) and were annealed for 10 h at 500 °C. Cubic GaN layers were deposited at 720 °C directly on 3C-SiC substrates. The adsorption and desorption of metal (Ga) layers on the c-GaN surface was investigated using the intensity of a reflected high energy electron beam (RHEED) as a probe. The structural and morphological properties of both the 3C-SiC substrates and the group III-nitride epilayers were measured by high resolution X-ray diffraction (HRXRD) and atomic force microscopy (AFM).

Reciprocal space mapping (RSM) has been performed to determine the content of hexagonal inclusions and strain in the epilayers.

As an important step to improve the GaN surface morphology in a systematic way, it is essential to understand the surface structure and the underlying growth process on an atomic scale. In particular, the kinetic processes of adsorption and desorption on the surface are considered as key parameters that govern the surface morphology, incorporation kinetics and consecutively the overall material quality. In MBE of GaN, two-dimensional surfaces are commonly achieved under Ga-rich conditions, with theoretical [24] and experimental [25, 26] evidence suggesting that the growth front is stabilized by a metallic Ga adlayer. The optimum conditions for the epitaxial growth of c-GaN are mainly determined by two parameters, the surface stoichiometry and the substrate temperature [22]. Both parameters are interrelated; therefore an in situ control of substrate temperature and surface stoichiometry is highly desirable. The study of the surface reconstruction by RHEED was one of the key issues in understanding the c-III nitride growth [22, 27, 28]. First principle calculations by Neugebauer et al. [29] show that all energetically favored surface modifications of the nonpolar (001) c-GaN surface are Ga-stabilized and therefore optimum growth conditions are expected under slightly Ga-rich conditions.

By recording the RHEED intensity transient of the (0,0) reflexion of the (2×2) reconstruction the Ga-coverage in the range between 0 and 1 monolayer can be estimated with an accuracy of 0.1 monolayer [9]. Optimum growth conditions of c-III nitrides were found, when a one monolayer Ga coverage is formed at the growing surface [9]. This is in contrast to what has been observed with h-GaN, where the optimum growth conditions with regard to surface morphology are related to the formation of a Ga bilayer (c-plane, [30, 31]) or a trilayer (m-plane, [26]), respectively. Under one monolayer Ga coverage the root mean square (RMS) roughness of the c-GaN surface measured by a $5 \times 5 \mu\text{m}^2$ AFM-scan is decreasing to a minimum value of 2.5 nm. The smoother the surface of the epilayer the narrower is also the rocking curve line width (ω -scan) of the cubic GaN and the higher is the structural quality of the cubic epilayer.

In Fig. 15.4 the rocking curve line width (ω -scan) of all our cubic GaN epilayers (full triangles) grown on 3C-SiC is plotted versus c-GaN layer thickness. Two clear effects can be seen from this plot. First a reduction of the full width at half maximum (FWHM) with increasing epilayer thickness is observed. This linewidth dependence is consistent with the defect annihilation process observed in c-GaN grown on GaAs (001) substrates [32]. Since in zinc-blende structure the stacking faults (SFs) lie on the (111) planes, an annihilation mechanism is possible, when two SFs, lying, for example on the (111) and on the (-1-11) planes intersect and annihilate simultaneously with the creation of a sessile dislocation aligned along [110] directions. For the case of 3C-SiC, where the lattice mismatch is only -3.5% to c-GaN, the full line shows the theoretical calculated FWHM as a function of layer thickness using the dislocation glide model by Ayers [33]. This model implies that the dislocation density N_{disl} is inversely proportional to the layer thickness d and that the FWHM is proportional to $d^{-1/2}$. Comparing the full curve with the experimental data (full triangles) a reduction of the FWHM by a factor 1.5 is still possible. For the sake

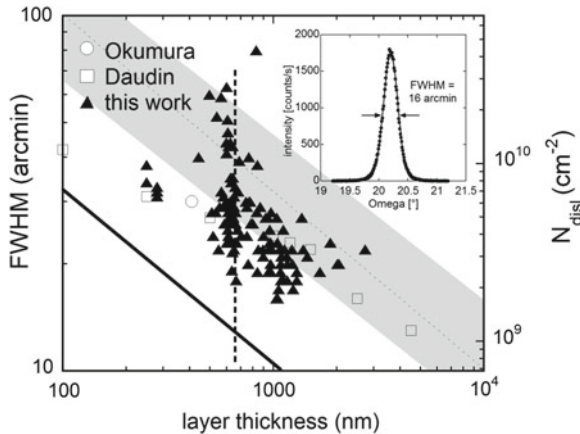


Fig. 15.4 Rocking curve linewidth of cubic GaN epilayers grown on 3C-SiC substrates versus thickness of the cubic GaN epilayers

of completeness the shaded area in Fig. 15.4 depicts the range of FWHM values as measured for cubic GaN grown on GaAs substrates. By comparing our data with data cited in literature, the dependence of the FWHM on film thickness has to be taken into account. Up to now, only two other groups reported data on 3–5 μm thick 3C-SiC/Si (001) pseudosubstrates grown by chemical vapor deposition (open circle Ref. [34] and open squares Ref. [35]). As can be seen in Fig. 15.4 we are clearly able to remain under the best cited values, indicating the improved structural quality of our c-GaN epilayers due to the availability of free standing, bulk like 3C-SiC (001) substrates. These experiments were performed on freestanding 3C-SiC (001) substrates, however, similar results were also obtained on 10 μm thick 3C-SiC (001) grown on Si (001) substrates (not included in Fig. 15.4).

As mentioned above, the second parameter which strongly influences the quality of the cubic epilayers is the roughness of the 3C-SiC substrate. In Fig. 15.4 the rocking curve linewidth of 600 nm thick c-GaN epilayers varies from 60 to 20 arcmin for 3C-SiC substrates with different surface roughness (indicated by the vertical dashed line). The RMS-roughness of the corresponding 3C-SiC substrates as measured by AFM on $5 \times 5 \mu\text{m}^2$ large areas varied between 11 and 0.7 nm, respectively. The smoother the surface of the substrates the narrower is the FWHM and the higher is the structural quality of the cubic epilayer. This observation is in agreement with measurements of Ref. [34] and indicates that a further improvement of the surface preparation (atomic flat surfaces) may allow to achieve the theoretical limit indicated by the full line.

However, using the method of Gay et al. [11], which correlates the X-ray FWHM with the dislocation density, one sees from Fig. 15.4, that even with the best surface roughness a residual dislocation density in the order of $N_{\text{disl}} \sim 10^9/\text{cm}^2$ remains for about 1 μm thick c-GaN epilayers. For many device applications such a high density of dislocations severely reduces the device performances and it is urgently demanded to avoid them. As discussed above, nanoheteroepitaxy offer this possibility

and avoids the defect generation when the substrate nanostructures have a size of about 40 nm.

15.4.2 Molecular Beam Epitaxy of Selective-Area-Grown Cubic GaN

The optimized growth conditions of cubic GaN described above are the basis for the growth of cubic GaN on prepatterned 3C-SiC/Si (001) substrates by MBE. Pre patterning of the substrate was achieved, i.e., by NSL (see Sect. 15.3), which offers a large area of a patterned substrate surface. Due to the large-patterned area it is guaranteed that the electron beam for RHEED touches the patterned surface and monitors information about the selective-area-growth of cubic GaN. Therefore, we discuss MBE growth only for substrates patterned by NSL.

On the patterned 3C-SiC/Si (001) substrate displayed in Fig. 15.2 a 440 nm c-GaN (001) thin film was grown [36]. For comparison a reference sample with a c-GaN epilayer of the same thickness was grown on an unstructured 3C-SiC substrate. For both patterned and unpatterned substrates the growth temperature was 720 °C and an one monolayer Ga coverage at the surface was used to grow under optimum conditions [9]. Figure 15.5a shows the RHEED pattern ([110] azimuth) of the planar cubic GaN layer of the reference sample. The long streaks indicate a two-dimensional surface. Figure 15.5b illustrates the [110] azimuth RHEED pattern of the surface of a 440 nm thin GaN layer grown on nanostructured 3C-SiC/Si (001). The RHEED pattern in Fig. 15.5b is similar to the one of the planar c-GaN layer clearly indicating the growth of c-GaN also on the prepatterned 3C-SiC. Obviously, the three-dimensional structure of the surface does not disturb the growth conditions in a way that would lead to the formation of hexagonal GaN. Figure 15.6a shows a side-view SEM image of the

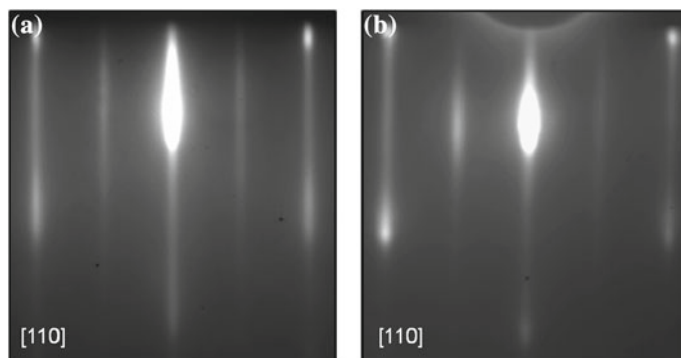


Fig. 15.5 **a** RHEED pattern of a 440 nm thin cubic planar GaN on 3C-SiC/Si (001), **b** RHEED pattern of a 440 nm thin cubic GaN layer grown on nanostructured 3C-SiC/Si (001) (both images in [110] azimuth) [36]

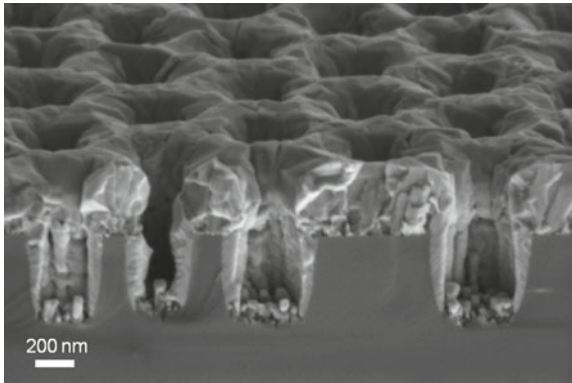


Fig. 15.6 Side view SEM image of a 440 nm cubic GaN layer grown on 3C-SiC/Si (001) nanopatterned by NSL

440 nm c-GaN on 3C-SiC/Si (001) nanopatterned by NSL. It is obvious from this image that there is GaN growth both on the SiC top surface and inside the SiC holes. The holes have not been closed by coalescence of the GaN top layer at this GaN layer thickness. The growth rate inside the holes is lower than on the (001) top surface due to geometrical effects. The large surface roughness at the bottom of holes observed before leads to a particularly grainy structure of the GaN film here.

15.5 Characterization of Selective-Area-Grown Cubic GaN

In Sect. 15.5, we shall discuss the characterization of the selective-area MBE grown c-GaN. HRXRD and cross-sectional transmission electron microscopy (XTEM) were used to characterize the structural properties. The optical properties were studied by microphotoluminescence (μ - PL) measurements.

15.5.1 Cubic GaN on 3C-SiC/Si (001) Substrate Prepatterned by Nanosphere Lithography

HRXRD is a powerful tool to characterize the strain distribution and defect densities in heteroepitaxially grown films. Figure 15.7 shows an asymmetrical reciprocal space map around the (113) reflection of the selectively grown 440 nm thin c-GaN film. Position 1 marks the bulk value of 3C-SiC [37]. Position 2 presents the literature value [38] of planar c-GaN and point 3 shows the experimental data of selective-area grown c-GaN, respectively. The selective-area-grown c-GaN is relaxed to the 3C-SiC with a minimal residual tensile strain. The reason for the residual tensile strain can

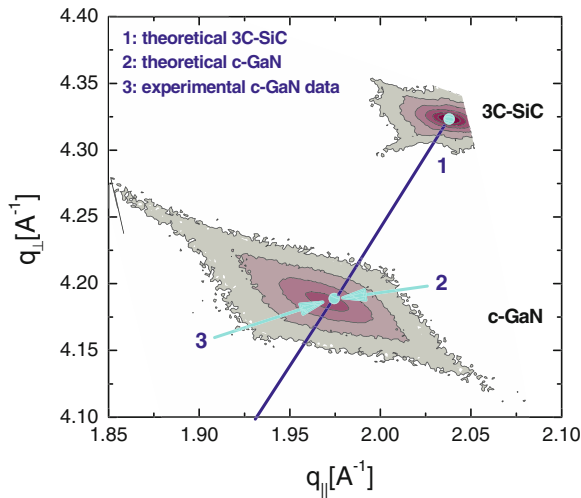


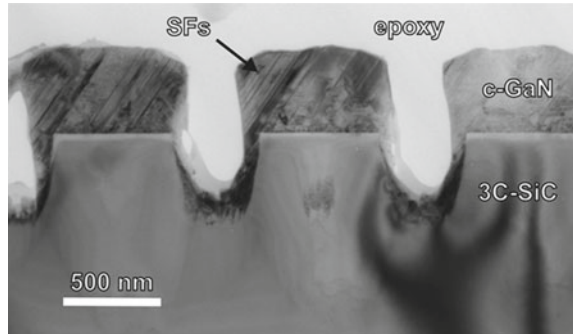
Fig. 15.7 Reciprocal space map around the (113) reflection of selective-area-grown c-GaN [36]

be found in the different thermal expansion coefficients of cubic GaN and 3C-SiC [39]. The same measurements were done for the planar reference layer and show that there is equal strain in both cases. The lattice parameter in growth direction was determined to $4.503 \pm 0.001 \text{ \AA}$. Additionally, a negligible amount of hexagonal inclusions in the selective-area-grown c-GaN is measured by symmetrical reciprocal space maps around the (002) reflection (not shown). The FWHM of the rocking curve of the selective-area-grown c-GaN is about 29 arcmin. and smaller than the FWHM of the rocking curve of the planar c-GaN reference layer with 36 arcmin. Using the method of Gay et al. [11] the defect density of selective-area-grown c-GaN is determined to be $4.5 \times 10^9/\text{cm}^2$ and $7.4 \times 10^9/\text{cm}^2$ for a planar layer. It should be noted that all HRXRD data measured on selective-area grown films are values averaging over the GaN top layer and the GaN at the sidewalls and bottoms of the SiC nanoholes.

In order to investigate the micro- and nano-structural features of the MBE grown GaN nanostructures, cross-sectional TEM samples were prepared by mechanical grinding and polishing followed by an ion beam thinning step. The samples were subsequently examined in a Philips CM200ST TEM operated at 200 kV.

Figure 15.8 shows a TEM bright-field micrograph of the nanostructured sample taken along the [110] zone axis under a two-beam condition. The cross section cuts through a row of $\sim 300 \text{ nm}$ deep and roughly 400 nm wide holes in the SiC substrate overgrown with about 400 nm GaN. Selective area diffraction (SAD) confirms that the GaN is cubic and is epitaxially oriented in full registry with the 3C-SiC/Si (001) substrate. The c-GaN film on the top SiC surface exhibits lateral facets which are inclined by $\sim 10^\circ$ with respect to the growth direction and additional facets on the top which are inclined by $\sim 20^\circ$ with respect to the sample template surface.

Fig. 15.8 Cross-sectional TEM image of a nanostructured cubic GaN film taken along the $[110]$ zone axis under two-beam condition. Stacking faults along the $[111]$ direction can be observed in the cubic GaN and are marked with ‘SFs’. [36]



Sanorpim et al. [40] have observed similar faceting of cubic GaN in their studies of epitaxial lateral overgrowth of (001)-oriented stripe-patterned GaAs with cubic GaN by MOVPE. The mechanism of facet formation is not yet fully understood and will be a topic of further studies.

The GaN film shown in Fig. 15.8 contains stacking faults (‘SFs’) mainly on the (111) planes. Due to the $[110]$ specimen orientation these stacking faults are seen edge on and therefore appear as bright and dark straight lines. In $[110]$ SAD patterns like the one in Fig. 15.9a taken from the middle island of Fig. 15.8 they lead to streaks along the $[111]$ direction. Additional streaks can be found along the $[111]$ direction but they are significantly weaker indicating a much lower stacking fault density on these planes. This is consistent with observations in weak-beam dark-field images (not shown) which also support an asymmetric stacking fault density. The same finding can be made in HRXRD symmetrical reciprocal space maps around the (002) reflection (not shown).

In addition to the reflections originating from cubic GaN and the stacking faults therein, weaker spots along the $[111]$ direction can be found. All these additional reflections can be explained by the formation of a small fraction of hexagonal inclusions, which are predominantly formed with their c -axis along the $[111]$ direction. Figure 15.9b shows the expected positions of reflections in a SAD pattern originating from cubic GaN (filled circles) and from hexagonal inclusions (crosses) as simulated using the JEMS code [41], assuming an epitaxial relationship of $[0002]_h\text{-GaN} \parallel [111]_c\text{-GaN}$ and $[110]_c\text{-GaN} \parallel [1120]_h\text{-GaN}$. The absence of similar diffraction spots along the $[111]$ direction indicates a negligible amount of hexagonal inclusions along this direction, in perfect agreement to a much smaller density of stacking faults on the (111) plane. This indicates that high stacking fault densities and hexagonal inclusions are correlated. While the contrasts in TEM bright-field images are dominated by stacking faults, it should be noted that there is also a limited number of dislocations close to the GaN/SiC interface, the density of which decreases over the first hundred nanometers.

The optical properties of the patterned cubic GaN layer were studied by room temperature μ – PL measurements. Luminescence was excited by the 325 nm line of a HeCd laser with a power of 400 μ W on the sample surface (beam diameter 1–2 μ m).

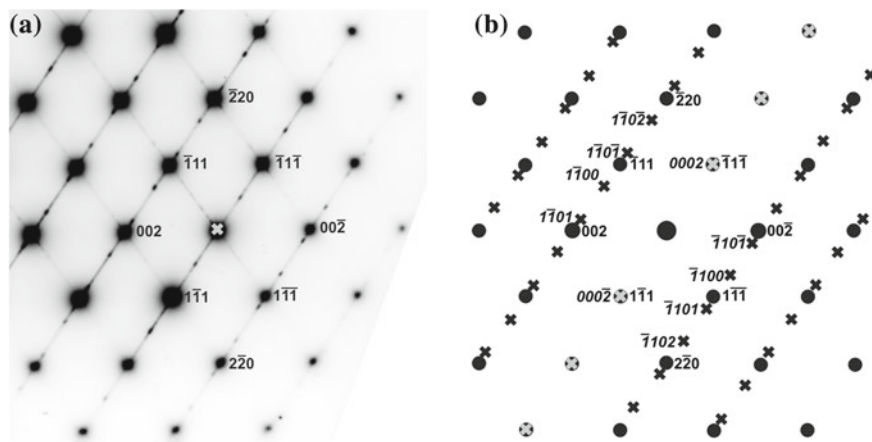


Fig. 15.9 **a** SAD pattern taken from the middle cubic GaN "island" in Fig. 15.8 along the $[110]$ cubic GaN zone axis with the main reflections indexed. Streaks along $[1\bar{1}1]$ and $[\bar{1}11]$ indicate the formation of stacking faults in these directions. **b** Simulated SAD pattern of cubic GaN along the $[110]$ direction (*filled circles*) together with the simulation of h-GaN viewed along the $[11\bar{2}0]$ direction (*crossed*). The good match of the experimental pattern (**a**) with the simulation (**b**) indicates the presence of a small fraction of hexagonal inclusions along the $[1\bar{1}1]$ direction within the cubic GaN "islands" [36]

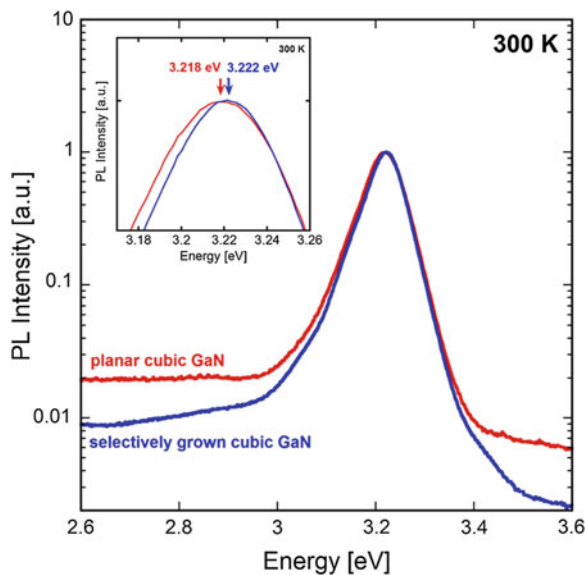


Fig. 15.10 Room temperature μ -PL spectra of a planar cubic GaN epilayer (*red*) and selective-area-grown c-GaN film (*blue*) [36]

In Fig. 15.10 the spectra of the c-GaN planar reference layer sample (red curve) and the selective-area-grown cubic GaN sample (blue curve) are depicted. The spectra show that there are no luminescence bands of the hexagonal phase indicating again that amount of hexagonal inclusions found by XTEM in our nanopatterned GaN is negligible.

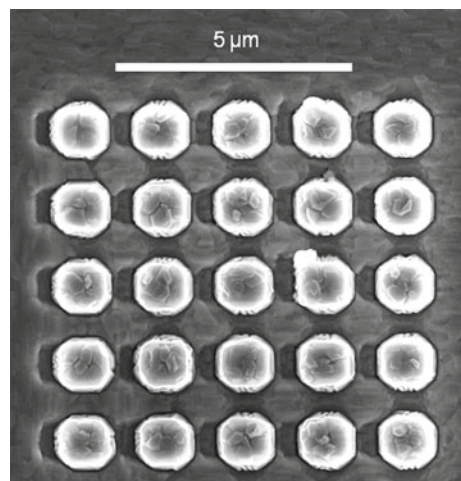
The peak of the band-edge luminescence of the reference layer is at 3.218 eV. This value agrees well with the literature value of 3.21 eV for cubic GaN grown on GaAs [42]. There is a blue shift of 4 meV in the band-edge transition (3.222 eV) of the selective-area-grown cubic GaN sample. The shift to a higher bandgap energy indicates that the tensile strain in the selective-area-grown cubic GaN that was shown by HRXRD is lower than in the planar cubic GaN layer.

15.5.2 Cubic GaN on 3C-SiC/Si (001) Substrate Prepatterned by Electron Beam Lithography

Figure 15.11 shows a SEM top view image of post-shaped 3C-SiC (001) nanostructures (see Fig. 15.3) overgrown with 400 nm c-GaN [21]. The edge length of the post structures is increased after GaN overgrowth from about 500 nm to about 1 μm . Furthermore there are darker areas in between neighboring posts, indicating deepenings in the GaN layer. They arise probably due to shadowing in particular when the sample holder rotation is stopped during MBE growth for RHEED inspection of the growth surface.

To have a closer look to the GaN on the post structures, cross-sectional TEM specimens were prepared using a focused ion beam (FIB) and analyzed using either a JEOL 2000 FX or a FEI Technai F20 microscope at 200 kV. Figure 15.12a displays

Fig. 15.11 Top view SEM image of a nanostructure array overgrown with 400 nm c-GaN [21]



a bright-field TEM micrograph of an individual 3C-SiC (001) post overgrown with 400 nm c-GaN taken along the $[110]$ zone axis. The GaN surface is covered with a Pt protection film (dark in Fig. 15.12a) necessary in the TEM preparation process. The image shows that the GaN grows on the top of the 3C-SiC post and on its sidewalls. Very generally speaking, we observed in this and all similar samples that GaN growth on the sidewalls is characterized by a huge irregularity of the stacking sequence in one of the $\langle 111 \rangle$ directions, while the stacking fault density in the c-GaN on top of the SiC posts is comparatively small. The GaN growth on the sidewalls of the 3C-SiC posts is dominated by $\{111\}$ planar defects. One reason for this could be the sidewall surface roughness resulting from the etching process during substrate patterning. Another reason is probably the deviation from an ideal 90° slope of the flanks. The GaN layer thickness on the sidewalls is smaller than on top of the post. Hence there is a lower GaN growth rate on the sidewalls than on top of the 3C-SiC post.

Since the TEM lamella in Fig. 15.12a was cut through the sidewall of the post and not through the center as sketched in Fig. 15.12b, the GaN is visible on three sidewalls of the post. This leads to the strongly varying contrasts within the upper

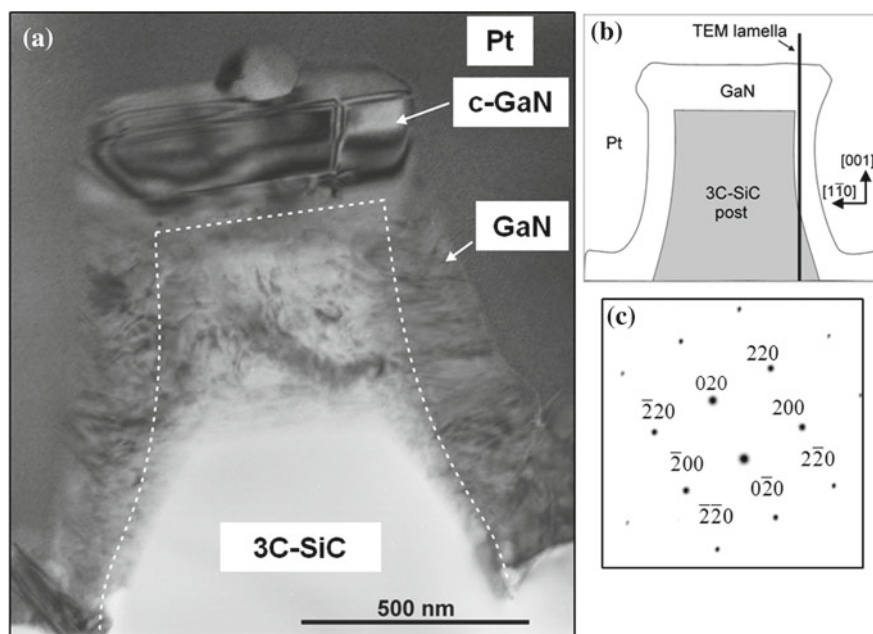


Fig. 15.12 **a** Cross-sectional TEM image of an individual 3C-SiC post overgrown with 400 nm cubic GaN taken along the $[110]$ zone axis. **b** A schematic cross-sectional view through the center of a typically overgrown SiC post parallel to the $[1\bar{1}0]$ direction. The TEM lamella cuts through the sidewall of the post perpendicular to the $[1\bar{1}0]$ direction. **c** SAD pattern (contrast inverted) taken from the middle cubic GaN island in (a) along the $[001]$ cubic GaN zone axis with the main reflections indexed [21]

part of the SiC post, since here the almost defect free crystal lattice of the SiC post is superimposed with the defect rich GaN growing on the flanks of posts. The GaN on the top of the post grows in individual crystals. It should be emphasized that the part of the GaN film displayed in Fig. 15.12a is located at the edge of the GaN top layer. The homogeneous contrasts within this part of the GaN film indicates a very low defect density of the GaN growing on top of the SiC post. There is only one dislocation like defect running vertically in the GaN top bit. The corresponding SAD pattern taken from the central GaN area on top of the post in Fig. 15.12a is shown in Fig. 15.12c. The diffraction pattern can be completely assigned to the lattice of cubic GaN with the [010] zone axis-oriented parallel to the electron beam. The SAD pattern contains no further reflections indicating the presence of a crystal with a pure cubic phase. These are the first steps toward defect-reduced cubic GaN grown via MBE on a dimensionally limited 3C-SiC (001) growth area. A small reservation is, however, that we also found a small misaligned GaN crystal centered on top of the epitaxial GaN film, not contributing to the SAD pattern shown.

15.6 Influences of the 3C-SiC/Si Substrate on the Selective-Area-Grown Cubic GaN

In addition to the defects discussed above, there is yet another class of defects originating from the SiC substrates. 3C-SiC/Si (001) substrates exhibit two types of antiphase domains (APDs) sharing equal parts of the growth surface. The presence of antiphase domains is due to the fact that the zinc blende structure of 3C-SiC is composed of two equivalent fcc lattices (shifted by $1/4$, $1/4$, $1/4$ with respect to each other) which are occupied by either one or the other atomic species. Thus both (001) or (111) growth surfaces can be either Si or C terminated, corresponding to the two different APDs. During the nucleation of 3C-SiC on an elementary Si substrate APDs are assumed to be formed at terraces on the Si surface. The C-face {111} plane has a lower surface energy and thus has a higher growth rate than the Si-face. [43] Our studies [44] show that GaN nucleation on 3C-SiC/Si (001) is governed by the APDs of the substrate and that the APDs are transferred into the GaN films. Thus, the presence of the APDs is independent of the GaN layer thickness [44]. More important, however, is that the two types of domains contain a largely different stacking fault density. [21]

In the following, we will discuss the influence of the antiphase domains in the 3C-SiC/Si substrate on a thick selective-area-grown c-GaN film [13]. In contrast to the former sections we chose here a large layer thickness of about $1.4\ \mu\text{m}$ to achieve a pronounced lateral growth and to promote the formation of surface facets.

Figure 15.13a shows a top view SEM image of the surface of a $1.4\ \mu\text{m}$ thick c-GaN layer grown on 3C-SiC/Si (001) nanopatterned using the NSL technique (see Sect. 15.3). Even though the film thickness is as large as $1.4\ \mu\text{m}$ the GaN film is still discontinuous and exhibits a close-packed array of residual holes. In the SEM

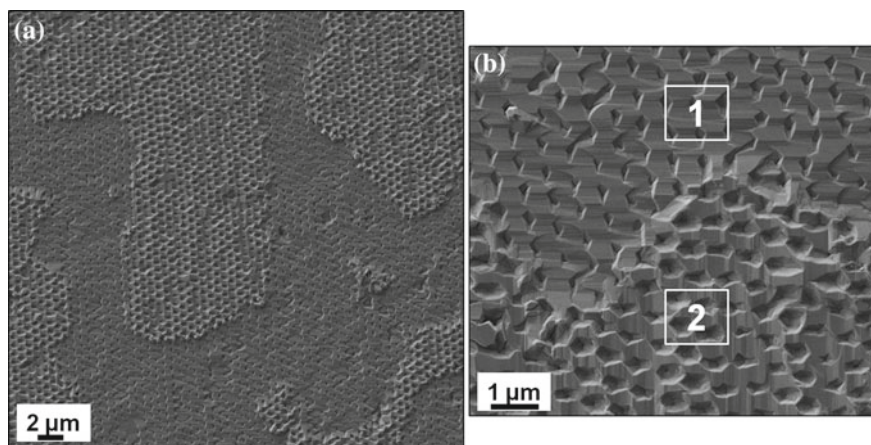


Fig. 15.13 **a** Top view SEM image of the surface of a $1.4\ \mu\text{m}$ thick cubic GaN layer grown on a NSL nano-patterned 3C-SiC/Si (001) substrate. The surface consists of domains, which have an arbitrary shape with lateral dimensions varying from a few micrometers up to about $100\ \mu\text{m}$. **b** Enlarged section of (a) showing the different size and orientation of residual holes in the two domains (1 and 2)

domains with an arbitrary shape with lateral dimensions varying from a few microns up to about $100\ \mu\text{m}$ can be seen. Different surface morphologies are present in the two types of domains, as is clearly visible in the detail SEM image of Fig. 15.13b. Note that the residual hole openings in domain 1 are smaller than in domain 2 and that their main axis is rotated by 90° with respect to each other in the two domains. NSL patterned surfaces may contain distortions of the periodicity (e.g., grain boundary-like mask defects) but a close inspection of the domains reveals that irregularities in the periodicity of the nanopattern on the substrate do not influence the surface morphology of the GaN grown within the same domain. This is an indication that the different morphologies originate from the domain structure of the substrate. The reason for these different GaN growth types is assumed to be differently terminated surfaces of the SiC substrate, leading to different polarities of the GaN film and thus a different growth behavior.

Figure 15.14 shows an AFM image of two adjacent domains on the surface of GaN grown on the prepatterned substrate. In domain 1 GaN grows with atomically smooth facets, indicating that in this region the Frank-Van-der-Merwe growth mechanism dominates. Due to the lateral growth the shape of the nanostructures changes from circular holes before GaN growth into triangle-shaped openings afterwards. The diameter of the holes is reduced from $500\ \text{nm}$ before to $100\text{--}200\ \text{nm}$ after GaN growth. In contrast to the layer-by-layer growth mechanism in domain 1, cubic GaN seems to grow in form of islands in domain 2 (Fig. 15.14). The shape of the holes after GaN growth has changed into squares with diameters from 200 to $350\ \text{nm}$.

The structural quality, averaged over all domains of the patterned cubic GaN film, is investigated by HRXRD measurements. Figure 15.15 shows a symmetrical reciprocal space map around the c-GaN (002) reflection. The FWHM of the (002)

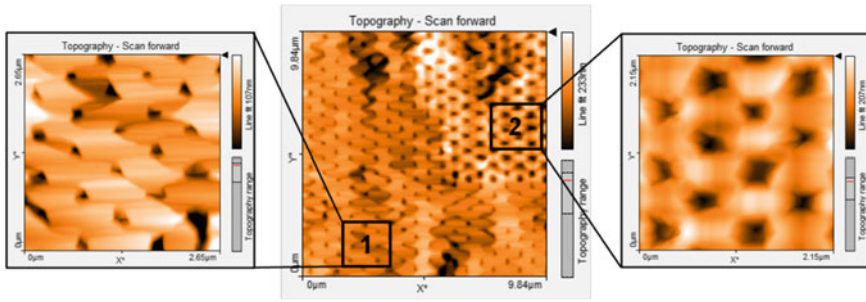
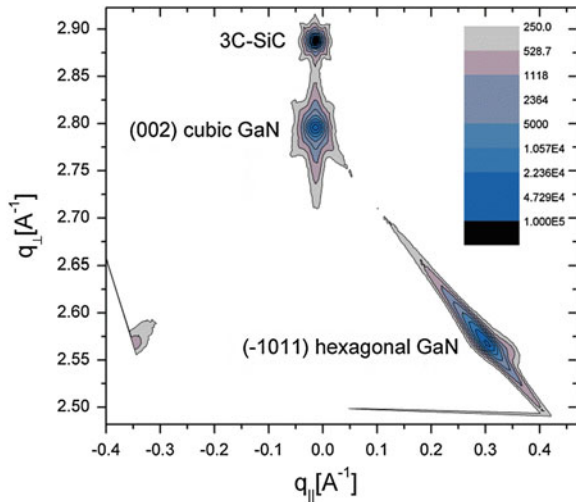


Fig. 15.14 AFM image of the surface of the selective-area-grown c-GaN with two adjacent domains. Zoom-in sections on the *left* and on the *right* show a step-flow-like flat surface in domain 1 and a more three-dimensional surface morphology in domain 2 [13]

Fig. 15.15 A symmetrical reciprocal space map around the (002) reflection of a selective-area-grown 1.4 μm thick GaN film on NSL prepatterned 3C-SiC/Si (001) [13]



rocking curve of the selective-area-grown cubic GaN is about 25 arcmin (compared to 29 arcmin in a 440 nm thin film). In addition to the (002) c-GaN reflection, there is a strong (-1011) reflection of hexagonal GaN visible in Fig. 15.15. From this, an amount of 78% hexagonal inclusions in the selective-area-grown cubic GaN is estimated. This value is very high compared to the cubic GaN reference layer, where only 17% hexagonal inclusions and a FWHM of the (002) rocking curve of 21 arcmin were observed at the same film thickness. Since the quality of the cubic phase of the selective-area-grown GaN and the reference layer are identical and in view of the enhanced formation of stacking faults on the side walls of SiC nanostructures (see Sect. 15.5) and since the hexagonal volume fraction in thin GaN films is negligible (see Sect. 15.5) it is concluded that substrate patterning enhances the formation of stacking faults and hexagonal inclusions mainly at the sidewalls, leading to substantial fractions of hexagonal GaN upon the growth of thick layers.

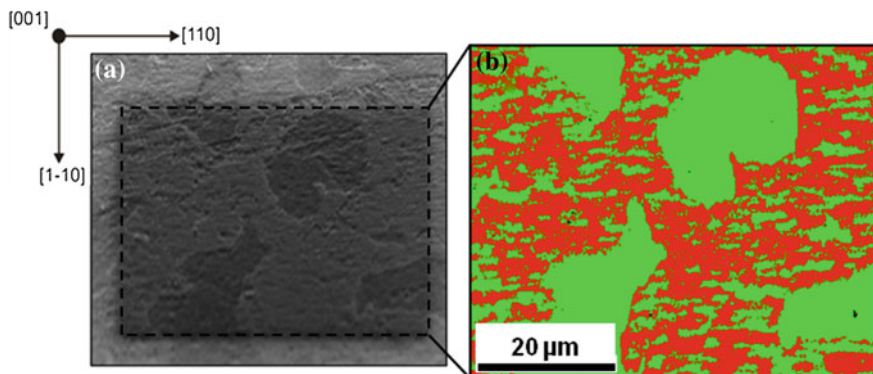


Fig. 15.16 **a** SEM image of the EBSD-measurement area on the surface of the $1.4\ \mu\text{m}$ thick selective-area-grown c-GaN film, which is tilted to about 70° in the measurement setup. **b** Phase map showing regions of predominantly cubic (*red*) and hexagonal (*green*) GaN [13]

Electron backscatter diffraction (EBSD) measurements were used for phase identification of the selective-area-grown GaN domains. For this method the primary electron beam ($20\ \text{keV}$) from a tungsten cathode of a XL40 ESEM is inelastically and elastically scattered by the crystal planes of the sample. This yields Kikuchi diffraction patterns, in which each pair of Kikuchi lines represents a crystal plane [45]. By this, areas of predominantly cubic and hexagonal phase of GaN can be distinguished and mapped. Figure 15.16a shows a top view SEM image of the EBSD-measurement area on the surface of the selective-area-grown c-GaN sample, which is tilted to about 70° in the microscope. The domains described above are clearly visible in this image. The diffraction pattern of the cubic and the hexagonal phase of GaN exemplify measured raw data and lead to the phase map in Fig. 15.16b. The crystal plane identification was achieved by a Hough-transformation followed by a least-square fit to both the cubic and the hexagonal phase, yielding a phase identification based on the smallest error. The data illustrated in the phase map were detected with a step size of $0.6\ \mu\text{m}$ and an angle resolution of $1\text{--}2^\circ$. The cubic phase is displayed in red color and the hexagonal phase of GaN in green, where a 50% threshold is used to assign either phase to a measurement position. That is, even though it is assumed that both phases are present in the domains, a sharp discrimination of the two pure phases is made in this diagram, and it obviously strongly correlates with the SEM image in Fig. 15.16a. It is clearly visible that the fraction of hexagonal phase between close-by domains varies. The domains with mainly cubic phase (red) contain hexagonal inclusions (green). Additionally there are domains where the hexagonal phase (green) dominates. The correlation between SEM images and AFM measurements demonstrates that in domains with smaller lateral growth the cubic phase is dominant. Furthermore, the domains with a smooth layer-by-layer growth can be identified to contain a high fraction of the hexagonal phase.

The optical properties of the domains of the selective-area-grown GaN layer were studied by room temperature $\mu\text{-PL}$ measurements. The spot diameter of this method is smaller than the domain size. In the inset of Fig. 15.17 a top view SEM image of the

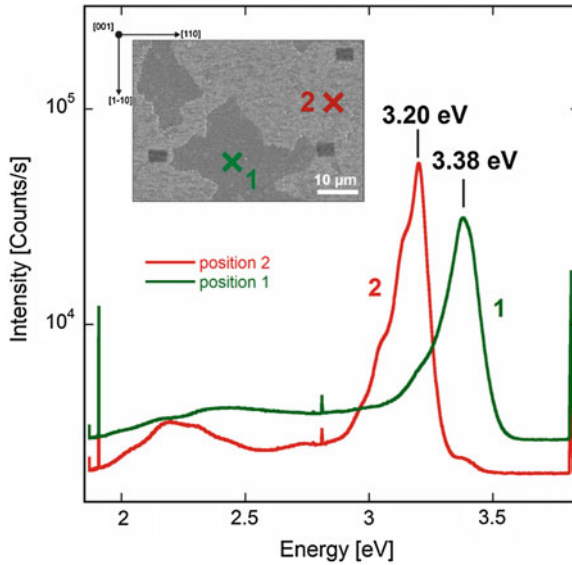


Fig. 15.17 Micro-PL spectra of adjacent domains (position 1 *green curve* and position 2 *red curve*) of the selective-area-grown cubic GaN at room temperature. *Inset: Top view SEM image of the μ – PL measurement area on the sample surface. Each domain is identified with markers (dark rectangles) positioned by a SEM [13]*

μ – PL measurement area on the sample surface is displayed. The different domains show a different secondary electron yield and thus can be clearly distinguished. In order to find appropriate positions in the optical measurements, contamination markers (dark rectangles in the inset of Fig. 15.17) were deposited with a SEM. Position 1 (green) is allocated to a domain which according to EBSD results is mainly hexagonal GaN, while position 2 (red) marks a domain consisting mainly of cubic GaN.

The μ – PL luminescence was excited by the 325 nm line of a HeCd laser with a power of 5 mW (beam diameter 1 μ m). The spectra of two domains (position 1 green curve and position 2 red curve) of the selective-area-grown GaN are depicted in Fig. 15.17. The band-edge luminescence of position 1 (green curve) is at 3.38 eV and is assigned to defect luminescence related to the hexagonal phase. It should be noted that a pure hexagonal phase is expected to show a luminescence peak at 3.42 eV, which would be clearly separated from the peak observed here. By comparison, the μ – PL peak of domain 2 has more intensity and occurs at 3.20 eV. This value agrees well with the band-edge transition at 3.21 eV for cubic GaN grown on GaAs [42]. Furthermore there is an emission shoulder with low intensity at 3.38 eV, which is an indication for defects and hexagonal inclusions in the selective-area-grown cubic GaN. A further luminescence peak in the red curve at 2.23 eV is related to defect luminescence. These spectra demonstrate clearly that in addition to the structural differences shown by EBSD the optical properties between two adjacent domains are quite different.

15.7 Cubic GaN/AlN Multi-Quantumwells on 3C-SiC Nanostructures

Due to the large band discontinuity between AlN, GaN and InN, these materials are qualified for novel nitride devices like quantum well infrared photodetectors (QWIP) and quantum cascade lasers (QCL). In the cubic system Zainal and coworkers [46] have shown a resonant tunneling through cubic GaN/AlGaN double barriers on GaAs substrate. Furthermore, Mietze et al. [47] demonstrated resonant tunnel diodes with reproducible I–V characteristics and recoverable negative differential resistance (NDR) based on Al(Ga)N/GaN double barrier structures on 3C-SiC (001).

The first basic steps toward nanoscale devices without any etching process are the growth of cubic AlN/GaN multiquantum wells (MQWs) on prepatterned 3C-SiC/Si (001) substrates by means of MBE. Growth conditions are based on the experimental data in Sect. 15.4 and ref. [47]. The substrate patterning has been realized by electron beam lithography and a reactive ion etching process using the same parameters as described in Sect. 15.3. The sample structure consists of 10 periods of 2 nm c-AlN barriers with a 4 nm c-GaN layer in between, which were grown on 3C-SiC post-shaped nanostructures. The 3C-SiC posts have a length of about 550 nm and a height of about 700 nm. Figure 15.18 displays cross-sectional TEM images of an individual 3C-SiC post overgrown with 10 periods of c-AlN/GaN MQWs taken along the [110] zone axis. Due to the difference in extinction lengths the c-GaN layers (dark) and the c-AlN barriers (bright) can be clearly separated. In general the sequential arrangement of the MQWs shows an undulated form, resulting from the high density of stacking faults. In regions without any {111} planar defects a straight sequential arrangement of c-AlN and c-GaN is observed. However, bunches of {111} stacking faults occur at which the growth rate is reduced leading to the undulating shape. The stacking

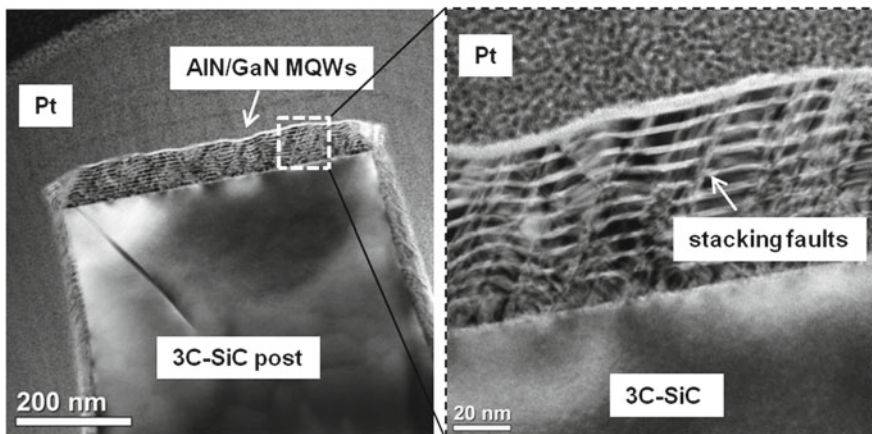


Fig. 15.18 Cross-sectional TEM images of an individual 3C-SiC post overgrown with 10 periods of c-AlN/GaN MQWs taken along the [110] zone axis

faults originate from the 3C-SiC/AlN interface and propagate towards the surface, accompanied by an increasing amplitude of the multilayer undulation.

These are first experimental results of cubic AlN/GaN MQWs grown on 3C-SiC nanostructures. We have shown that it is possible to grow cubic AlN/GaN MQWs on prepatterned substrates by MBE. It is obvious, however, that similar to pure c-GaN layers on prepatterned SiC substrates, the biggest challenge will be the elimination of the high stacking fault density. A possible approach is the reduction of the growth area to less than $100 \times 100 \text{ nm}^2$ towards nanoheteroepitaxy to reduce the density of crystalline defects and to avoid the undulated shape of the MQWs.

15.8 Conclusions

We conclude that the heteroepitaxy of nonpolar c-GaN on prepatterned substrates is a promising method for developing the structural quality of cubic nitrides. Our studies have shown that it is possible to grow phase-pure c-GaN on 3C-SiC nanostructures under Ga-rich growth conditions via MBE. Nanopatterning of the 3C-SiC/Si (001) substrate surface was realized by NSL and EBL followed by an RIE etching process. With both techniques different types of 3C-SiC nanostructures have been fabricated.

The selective-area-grown GaN, which was deposited on a surface patterned by NSL, crystallizes in the zincblende structure. HRXRD measurements exhibit that the selective-area-grown cubic GaN as well as planar epilayers are relaxed on 3C-SiC/Si (001) with a minimal residual tensile strain. The selective-area-grown cubic GaN displays lateral facets which are evidenced by cross-sectional TEM measurements. The GaN “islands” show stacking faults and a small fraction of hexagonal inclusions. Micro-PL measurements at room temperature demonstrate that the selective-area-grown cubic GaN is less tensile strained than a planar reference layer.

Not only stacking faults but also antiphase domains of the substrate influence the structural quality of the selective-area-grown c-GaN. The c-GaN grows in two different domains. The nanopatterning of the substrate does not influence the shape of these domains. HRXRD measurements show that at large layer thicknesses the hexagonal fraction in selective-area-grown cubic GaN is strongly enhanced. Several independent measurement techniques reveal that there is a largely differing amount of hexagonal inclusions and defects in the two sets of domains. Depending on the fraction of cubic or hexagonal phase the Volmer-Weber or the Frank-Van-der-Merwe growth mechanism dominates and the lateral growth rate varies accordingly.

Another focus lies on cubic GaN crystals on top of post shaped 3C-SiC nanostructures, fabricated by EBL and a RIE etching process. We have demonstrated that they grow nearly defect-free with excellent structural properties. Here the nanostructures are aligned parallel and perpendicular to the [110] directions of the substrate. On the sidewalls of these posts, however, the GaN layer contains a high density of {111} planar defects.

Moreover, a complex cubic AlN/GaN MQW layer structure on prepatterned 3C-SiC substrate has been successfully realized. However, the sequential arrangement of the MQWs shows an undulated form due to the high stacking fault density.

All in all the reduction of the stacking fault density must be the main issue of further studies. In order to draw a conclusion about the possibility of a defect reduction in GaN and the AlN/GaN MQW films on nanostructured surfaces according to the theory of nanoheteroepitaxy the size of the nanostructures still has to be scaled down further.

Acknowledgments The authors would like to thank L. Hiller, Th. Stauden and J. Pezoldt (TU Ilmenau) for patterning the substrates with electron beam lithography and reactive ion etching. The authors also wish to thank Th. Niendorf, K. Duschik and H.-J. Maier (University of Paderborn) for EBSD and some of the TEM measurements. We thank M. Ruth and C. Meier (University of Paderborn) for the micro-photoluminescence measurements. Furthermore we thank the team of the Ernst Ruska-Centre for Microscopy and Spectroscopy with Electrons (ER-C) at Forschungszentrum Jülich, in particular D. Meertens, M. Luysberg and K. Tillmann for access to and comprehensive support at the FIB and TEM facilities of ER-C. Part of the work at Paderborn was financially supported by German Science Foundation (As(107/4-1)).

References

1. Nakamura, S., Mukai, I., Senok, M.: Candela-class high-brightness InGaN/AlGaIn double-heterostructure blue-light emitting diodes. *Appl. Phys. Lett.* **64**, 1687 (1994)
2. Rajan, S., Waltereit, P., Poblenz, C., Heikman, S.J., Green, D.S., Speck, J.S., Mishra, U.K.: Power Performance of AlGaIn-GaN HEMTs Grown on SiC by Plasma-Assisted MBE. *IEEE Electron Device Lett.* **25**, 247 (2004)
3. Tschumak, E., Granzer, R., Lindner, J.K.N., Schweiz, F., Lischka, K., Nagasawa, H., Abe, M., As, D.J.: Nonpolar cubic AlGaIn/GaN heterojunction field-effect transistor on Ar-implanted 3C-SiC (001). *Appl. Phys. Lett.* **96**, 253501 (2010)
4. Fitzgerald, E.A., Watson, G.P., Proano, R.E., Ast, D.G.: Nucleation mechanisms and the elimination of misfit dislocations at mismatched interfaces by reduction in growth area. *J. Appl. Phys.* **65**, 2220 (1989)
5. Zubia, D., Hersee, S.D.: The Application of nanostructuring and substrate compliance to the heteroepitaxy of mismatched semiconductor materials. *J. Appl. Phys.* **85**, 6492 (1999)
6. Ambacher, O., Majewski, J., Miskys, C., Link, A., Hermann, M., Eickhoff, M., Stutzmann, M., Bernardini, F., Fiorentini, V., Tilak, V., Schaff, B., Eastman, L.F.: Pyroelectric properties of Al(In)GaIn/GaN hetero- and quantum well structures. *J. Phys. Condens. Matter* **14**, 3399–3434 (2002)
7. Bernardini, F., Fiorentini, V., Vanderbilt, D.: Spontaneous polarization and piezoelectric constants of III-V nitrides. *Phys. Rev. B* **56**, R10 024 (1997)
8. Waltereit, P., Brandt, O., Trampert, A., Grahn, H.T., Menninger, J., Reiche, M., Ploog, K.H.: Nitride semiconductors free of electrostatic fields for efficient white light-emitting diodes. *Nature* **406**, 865 (2000)
9. Schörmann, J., Potthast, S., As, D.J., Lischka, K.: In situ growth regime characterization of cubic GaN using reflection high energy electron diffraction. *Appl. Phys. Lett.* **90**, 041918 (2009)
10. Novikov, S.V., Stanton, N.M., Champion, R.P., Foxon, C.T., Kent, A.J.: Free-standing zinc-blende (cubic) GaN layers and substrates. *J. Crystal Growth* **310**, 3964 (2008)
11. Gay, P., Hirsch, P.B., Kelly, A.: The estimation of dislocation densities in metals from x-ray data. *Acta Metallurgica* **1**, 315 (1953)

12. DeCuir Jr, E.A., Manasreh, M.O., Tschumak, E., Schörmann, J., As, D.J., Lischka, K.: Cubic GaN/AlN multiple quantum well photodetector. *Appl. Phys. Lett.* **92**, 201910 (2008)
13. Kemper, R.M., Häberlein, M., Schupp, T., Weigl, M., Bürger, M., Ruth, M., Meier, C., Niendorf, T., Maier, H.J., Lischka, K., As, D.J., Lindner, J.K.N.: Formation of defects in cubic GaN grown on nano-patterned 3C-SiC (001). *Phys. Stat. Sol. (c)* **9**(3–4), 1028 (2012)
14. Sun, X.Y., Bommenna, R., Burckel, D., Frauenglass, A., Fairchild, M.N., Brueck, S.R.J., Garrett, G.A., Wraback, M., Hersee, S.D.: Defect reduction mechanisms in the nanoheteroepitaxy of GaN on SiC. *J. of Appl. Phys.* **95**, 1450 (2004)
15. Haynes, C.L., Van Duyne, R.P.: A versatile nanofabrication tool for studies of size-dependent nanoparticle optics. *J. Phys. Chem. B* **105**(24), 5599–5611 (2001)
16. Chassagne, T., Leycuras, A., Balloud, C., Arcade, P., Peyre, H., Juillaguet, S.: Investigation of 2 inch SiC layers grown in a resistively-heated LP-CVD reactor with horizontal hot-walls. *Mater. Sci. Forum* **457–460**, 273–276 (2004)
17. Cicero, G., Catellani, A., Galli, G.: Interaction of Water Molecules with SiC(001) Surfaces. *J. Phys. Chem. B* **108**, 16518 (2004)
18. Lindner, J.K.N., Seider, C., Fischer, F., Weigl, M., Stritzker, B.: Regular surface patterns by local swelling induced by He implantation into silicon through nanosphere lithography masks. *Nucl. Instr. Meth. B* **267**, 1394 (2009)
19. Gogel, D., Weigl, M., Lindner, J.K.N., Stritzker, B.: Plasma modification of nanosphere lithography masks made of polystyrene beads. *J. Optoelectron. Adv. Mater.* **12**, 740 (2010)
20. Hiller, L., Stauden, T., Kemper, R.M., Lindner, J.K.N., As, D.J., Pezoldt, J.: ECR-etching of submicron and nanometer sized 3C-SiC(100) mesa structures. *Mater. Sci. Forum* **717–720**, 901 (2012)
21. Kemper, R.M., Hiller, L., Stauden, T., Pezoldt, J., Duschik, K., Niendorf, T., Maier, H.J., Meertens, D., Tillmann, K., As, D.J., Lindner, J.K.N.: Growth of cubic GaN on 3C-SiC/Si (001) nanostructures. *J. Cryst. Growth* (2012). doi:[10.1016/j.jcrysgro.2012.10.011](https://doi.org/10.1016/j.jcrysgro.2012.10.011)
22. As, D. J.: Growth and characterization of MBE-grown cubic GaN, $\text{In}_x\text{Ga}_{1-x}\text{N}$, and $\text{Al}_y\text{Ga}_{1-y}\text{N}$. In: Manasreh, M.O. (ed.) *Optoelectronic Properties of Semiconductors and Superlattices*, Vol. 19, Chap. 9, pp. 323–450. Taylor and Francis, New York (2003)
23. As, D.J., Potthast, S., Schörmann, J., Li, S.F., Lischka, K., Nagasawa, H., Abe, M.: Molecular Beam Epitaxy of Cubic Group III-Nitrides on free-standing 3C-SiC substrates. *Mater. Sci. Forum* **527**, 1489 (2006)
24. Northrup, J.E., Neugebauer, J., Feenstra, R.M., Smith, A.R.: Structure of GaN (0001): The laterally contracted Ga bilayer model. *Phys. Rev. B* **61**, 9932 (2000)
25. Koblmüller, G., Brown, J., Averbek, R., Riechert, H., Pongratz, P., Speck, J.S.: Continuous evolution of Ga adlayer coverages during plasma-assisted molecular-beam epitaxy of (0001) GaN. *Appl. Phys. Lett.* **86**, 041908 (2005)
26. Brandt, O., Sun, Y.J., Däweritz, L., Ploog, K.H.: Ga adsorption and desorption kinetics on M-plane GaN. *Phys. Rev. B* **69**, 165326 (2004)
27. Schikora, D., Hankeln, M., As, D.J., Lischka, K., Litz, T., Waag, A., Buhrow, T., Henneberger, F.: Epitaxial growth and optical transitions of cubic GaN films. *Phys. Rev. B* **54**, 8381 (1996)
28. Feuillet, G., Hamaguchi, H., Ohta, K., Hacke, P., Okumura, H., Yoshida, S.: Arsenic mediated reconstructions on cubic (001) GaN. *Appl. Phys. Lett.* **70**, 1025 (1997)
29. Neugebauer, J., Zywiets, Z., Scheffler, M., Northrup, J.E., Van der Walle, C.G.: Clean and As-Covered Zinc-Blende GaN (001) Surfaces: Novel Surface Structures and Surfactant Behavior. *Phys. Rev. Lett.* **80**, 3097 (1998)
30. Mula, G., Adelman, C., Moehl, S., Oullier, J., Daudin, B.: Surfactant effect of gallium during molecular-beam epitaxy of GaN on AlN (0001). *Phys. Rev. B* **64**, 195406 (2001)
31. Adelman, C., Brault, J., Jalabert, D., Gentile, P., Mariette, H., Mula, G., Daudin, B.: Dynamically stable gallium surface coverages during plasma-assisted molecular-beam epitaxy of (0001) GaN. *J. Appl. Phys.* **91**, 9638 (2002)
32. Nagayama, A., Sawada, H., Takuma, E., Katayama, R., Onabe, K., Ichinose, H., Shiraki, Y.: Structural study on stacking faults in GaN/GaAs (001) heterostructures. *Inst. Phys. Conf. Ser.* **170**, 749 (2002)

33. Ayers, J.E.: New model for the thickness and mismatch dependencies of threading dislocation densities in mismatched heteroepitaxial layers. *J. Appl. Phys.* **78**, 3724 (1995)
34. Okumura, H., Ohta, K., Feuillet, G., Balakrishnan, K., Chichibu, S., Hamaguchi, H., Hacke, P., Yoshida, S.: Growth and characterization of cubic GaN. *J. Cryst. Growth* **178**, 113 (1997)
35. Daudin, B., Feuillet, G., Hübner, J., Samson, Y., Widmann, F., Philippe, A., Bru-Chevallier, C., Guillot, G., Bustarret, E., Bentoumi, G., Deneuve, A.: How to grow cubic GaN with low hexagonal phase content on (001) SiC by molecular beam epitaxy. *J. Appl. Phys.* **84**, 2295 (1998)
36. Kemper, R.M., Weigl, M., Kemper, R.M., Weigl, M., Mietze, C., Häberlen, M., Schupp, T., Tschumak, E., Lindner, J.K.N., Lischka, K., As, D.J.: Growth of cubic GaN on nano-patterned 3C-SiC/Si (001) substrates. *J. Cryst. Growth* **323**, 84 (2011)
37. Taylor, A., Jones, R.M.: The crystal structure and the thermal expansion of cubic and hexagonal silicon carbide, *Silicon Carbide-A High Temperature Semiconductor*, edited by J.R.O Connor, J. Smiltens, Oxford, Symposium Publications Division, Pergamon Press, 1960, Section III, Chap.1, p.147 (1960)
38. Strite, S., Juan, J., Li, Z., Salvador, A., Chen, H., Smith, D.J., Choyke, W.J., Morkoc, H., Vac, J.: An investigation of the properties of cubic GaN grown on GaAs by plasma-assisted molecular-beam epitaxy. *J. Vac. Sci. Technol.* **B9**(4), 1924 (1991)
39. Wu, J., Yaguchi, H., Zhang, B.P., Segawa, Y., Onabe, K., Shiraki, Y.: Optical properties of cubic GaN grown on 3C-SiC (100) substrates by metalorganic vapor phase epitaxy. *Phys. Stat. Sol. (a)* **180**, 403 (2000)
40. Sanorpim, S., Takuma, E., Ichinose, H., Katayama, R., Onabe, K.: Structural transition control of laterally overgrown c-GaN and h-GaN on stripe-patterned GaAs (001) substrates by MOVPE. *Phys. Stat. Sol. (b)* **244**(6), 1769 (2007)
41. Stadelmann, P.A.: EMS - A software package for electron diffraction analysis and HREM image simulation in materials science. *Ultramicroscopy* **21**(2), 131 (1987)
42. As, D.J., Schmilgus, F., Wang, C., Schöttker, B., Schikora, D., Lischka, K.: The near band edge photoluminescence of cubic GaN epilayers. *Appl. Phys. Lett.* **70**, 1311 (1997)
43. Nagasawa, H., Abe, M., Yagi, K., Kawahara, T., Hatta, N.: Fabrication of high performance 3C-SiC vertical MOSFETs by reducing planar defects. *Phys. Stat. Sol. (b)* **245**(7), 1272–1280 (2008)
44. Kemper, R.M., Schupp, T., Häberlen, M., Niendorf, T., Maier, H.-J., Dempewolf, A., Bertram, F., Christen, J., Kirste, R., Hoffmann, A., Lindner, J., As, D.J.: Anti-phase domains in cubic GaN. *J. Appl. Phys.* **110**, 123512 (2011)
45. Reimer, L.: *Scanning Electron Microscopy*, 2nd edn, pp. 368–374. Springer, New York (1998)
46. Zainal, N., Novikov, S.V., Mellor, C.J., Foxon, C.T., Kent, A.J.: Current-voltage characteristics of zinc-blende (cubic) Al_{0.3}Ga_{0.7}N/GaN double barrier resonant tunneling diodes. *Appl. Phys. Lett.* **97**, 112102 (2010)
47. Mietze, C., Lischka, K., As, D.J.: Current-voltage characteristics of cubic Al(Ga)N/GaN double barrier structures on 3C-SiC. *Phys. Stat. Sol. (a)* **209**(3), 439 (2012)